Nanoencapsulation and Stabilization of Single-Molecule/Particle Electronic Nanoassemblies Using Low-Temperature Atomic Layer Deposition

Jeong-Seok Na,[†] Jennifer A. Ayres,[‡] Kusum L. Chandra,[‡] Christopher B. Gorman,[‡] and Gregory N. Parsons[†,*]

Department of Chemical and Biomolecular Engineering and Department of Chemistry, North Carolina State University, Raleigh, North Carolina 27695

Received: July 25, 2008; Revised Manuscript Received: October 9, 2008

This work addresses a significant challenge in engineered molecular systems regarding both understanding and controlling the stability of molecule/nanoparticle nanostructures under ambient exposure. Results deal specifically with molecular electronic junctions, where electronic contacts and transport are known to be sensitive to sample history and ambient exposure. We demonstrate that low-temperature atomic layer deposition can gently encapsulate and stabilize molecular electronic junctions, making it feasible to handle and transport junctions in air for many days with minimal change in electronic conduction. These findings indicate the potential for long-term stability of advanced synthetic nanoparticle/molecule nanoconstructs. For this study, conductivity through nanoparticle/molecule/nanoparticle junctions is analyzed and found to be consistent with nonresonant charge tunneling through a single or a small number of oligomeric phenylene ethynylene molecules in the electrical junction. The conductivity was stable in vacuum and inert gas, but under ambient exposure, the current initially decreased, then increased rapidly, followed by a slower rise, reaching a value exceeding 10 times larger than initially measured. After encapsulating functional devices using atomic layer deposition of aluminum oxide thin films at 30−50 °C, the junction showed conductance similar to the precoated values, and the current remained unchanged after more than 15 days under ambient exposure. The presence of the molecule junction after encapsulation was confirmed by the observed transition to Fowler−Nordheim tunneling and analysis of junction breakdown at high fields. The high conformality, precise thickness control, and low-temperature compatibility of the atomic layer deposition method make it uniquely qualified to stabilize and protect molecular junctions and systems.

Introduction

Synthetic and engineered nanomaterial architectures are of significant interest for advanced optical, electronic, and nanostructural systems. One outstanding challenge in engineered molecular systems is to understand and control the stability of the molecular structures under ambient exposure. This problem is particularly acute in the field of molecular electronic junctions, where electronic contacts and transport mechanisms can be highly sensitive to sample history and ambient exposure. Although the physical and chemical stabilities of molecular monolayers over extended periods (weeks to months) in ambient atmosphere have been investigated by many groups,[1,2] the stability of charge transport through isolated molecular junctions during extended ambient exposure is less widely characterized,[3] and methods to protect the junctions from the environment have been only briefly discussed.[4] Here, we demonstrate a novel method based on low-temperature, atomic layer, thin-film deposition to effectively encapsulate and isolate functional molecular electronic junctions, enabling long-term stable characterization. The ability to stabilize molecular junctions may give rise to new methods; for example, to construct stable organic/inorganic nanoframeworks or stabilize advanced molecular electronic circuitry.

The current versus voltage ($I-V$) characteristics of single or small groups of molecules have been extensively investigated[5,6] using break junctions,[7−9] scanning probe techniques,[10−12] and nanoparticle bridge structures.[13,14] An extension of the nanoparticle bridge involves formation of nanoparticle/molecule/nanoparticle structures, referred to here as "nanoparticle dimers",[15,16] and contacted across nanoscale metal electrodes. This approach is particularly attractive because (i) the molecules are covalently bound to the metal nanoparticles; (ii) the structure can, in principle, be amenable to parallel fabrication; (iii) the structures can be maintained electrically connected for long periods of time (days and weeks), enabling time- and temperature-dependent current to be characterized.

In this article, nanoparticle/molecule/nanoparticle structures, consisting of ∼40 nm gold nanoparticles linked by a single (or small number of) oligomeric phenylene ethynylene molecules (OPEs), were synthesized and electrically bridged across planar nanoscale electrode gaps.[16,17] The stability of the current through the junction was investigated and characterized upon exposure to ambient laboratory air and under alternate exposures to air and vacuum. To improve the ambient stability of the dimer, passivation of nanoparticle/molecule/nanoparticle structures was investigated using atomic layer deposition (ALD) of Al_2O_3. The ALD process involves sequential exposures of a sample to surface-saturating exposures of reactive precursors used in the deposition. For the case of Al_2O_3 ALD, trimethylaluminum and water vapors are typically used, and exposures are separated in time using Ar gas flow. Repeating the reactant exposure cycles

* Corresponding author. E-mail: parsons@ncsu.edu.
[†] Department of Chemical and Biomolecular Engineering.
[‡] Department of Chemistry, North Carolina State University, Raleigh, NC 27695.

10.1021/jp8066298 CCC: $40.75
Published on Web 11/24/2008

allows the resulting film thickness to be controlled with near monolayer precision. There are numerous reports describing the application of ALD Al_2O_3 for coating zirconia nanoparticles[18] and carbon nanotubes[19,20] and for passivation layers for organic light-emitting diodes.[21,22] It is well-known that ALD can form extremely continuous, uniform, and conformal films,[23] and Al_2O_3 films can be grown by ALD at temperatures below 100 °C.[24] The gold−sulfur (Au−S) bond is sufficiently strong that it is expected to remain stable under processing at moderate elevated temperatures,[25,26] allowing the coating process to not significantly modify the chemical structure of the molecule or molecule/metal contact. We report here initial detailed investigation results for low-temperature passivation of functional molecular electronic junctions using atomic layer deposition technology.

Results and Discussion

The nanoparticle/molecule/nanoparticle dimers were synthesized according to previously published methods[16,27] and utilized to form an electrical bridge across a planar nanogap electrode. We note that the dimer formation procedure[16,27] was performed under conditions in which the concentration of molecules and nanoparticles was controlled such that dimers were likely to contain only one or a small number of molecules. In fact, during the dimer formation process, when a higher concentration of molecules was used, significant agglomeration of nanoparticles was observed, consistent with more than one molecule on each nanoparticle surface.[15] Under conditions used for the dimer formation, the concentration of clusters of three or four nanoparticles was relatively low, further suggesting that many of the nanoparticle dimers contained only one or two molecules. An example transmission electron microscopic (TEM) image of an uncoated synthesized dimer, shown in Figure 1a, shows two nanoparticles with diameters of ∼40 nm separated by the length of an OPE linker molecule (∼2 nm). Figure 1b shows a plan-view scanning electron microscope image of a nanoscale Pd metal electrode gap of ∼70 nm fabricated by oblique angled metal evaporation, which is used to trap and electrically contact the nanoparticle/molecule/nanoparticle dimers, as shown in the scaled schematic in Figure 1c.

Typical current-vs-voltage curves measured for an example trapped molecular dimer are shown in Figure 2a, measured immediately after assembly in the nanogap, and after various exposure times to laboratory air. The shape of all the $I-V$ curves collected is consistent with nonresonant charge tunneling, as shown previously for these structures.[28] The current values measured between −0.2 and +0.2 V immediately after initial trapping correspond to a resistance of 4.8 ± 0.1 GΩ in the circuit. This value is within a factor of 2 of the value of ∼2.8 GΩ previously reported by our group for similar trapped OPE-linked gold nanoparticle dimers[16] and is also close to the value of 1.7 ± 0.4 GΩ reported at ± 0.1 V for a single molecule of OPE measured by scanning probe microscopy.[28] Further evidence of the number of molecules present can be obtained from surface enhanced Raman spectroscopy (SERS). Analysis of nanoparticle/molecule dimers previously fabricated with the same methods used here[29] showed temporal blinking in the concurrent SERS images, consistent with a single molecule between the nanoparticles. Other groups utilizing similarly prepared nanoparticle/molecule dimers also cited similar SERS results consistent with single-molecule behavior between the nanoparticles.[15]

The stability of the current through several nanoparticle/OPE/nanoparticle structures was investigated in vacuum and in ambient air, as shown in Figure 2. The stability under air exposure is shown in Figure 2a, d, and e. The data in Figure 2a shows results from a single dimer stored in laboratory air and measured in vacuum over a period of ∼25 days. The current was observed to rise as a function of time, but the shape of the I−V curve did not significantly change. Also shown in Figure 2a are I−V traces from a control experiment in which a relatively large (∼80 nm) gold nanoparticle was trapped between the nanogap electrodes following the same procedure used for dimer trapping. A much larger current was observed through the single nanoparticle, and the shape of the I−V trace through the single nanoparticle was more linear than for the nanoparticle/molecule dimer, as shown in Figure 2b. The current through the single nanoparticle was measured periodically over 18 days under laboratory air exposure, and the current increased by approximately a factor of 2 during that period. The gold nanoparticles are coated with a citrate capping layer, which may lead to some resistance at the nanoparticle/electrode connections. However, compared with the nanoparticle dimers, the much higher current through the single nanoparticle structures demonstrates that the electrode contact resistance contributed minimally (∼0.1%) to the overall measured resistance of the OPE-linked junction.

As another control experiment, Figure 2c shows the current measured at 0.5 V applied bias for a single dimer sample held in vacuum over a period of 12 days. A current near 1 nA was observed, and no measurable change in current was detected. The effect of applied bias on the stability of the I−V measurements was also evaluated. Samples were measured under vacuum for several hours with a continuous bias of 0.5−1 V applied, and no significant change in the current was observed.

Under air exposure, the dimer samples generally showed both short-term (over several minutes) and long-term instability (over

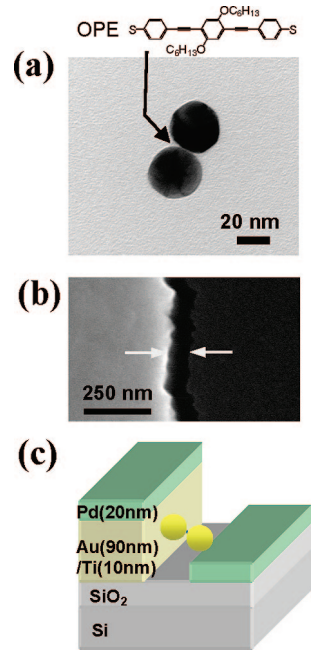

Figure 1. (a) Example TEM image of an oligomeric phenylene ethynylene molecule (OPE)-linked nanoparticle dimer, consisting of two gold nanoparticles with a diameter of ∼40 nm covalently connected by the molecule. The structure of the OPE molecule is also shown. (b) Plan-view SEM image of the nanogap electrode with a gap width of ∼70 nm, fabricated by oblique-angle metal evaporation with a tilt angle of 50° from the normal to the surface. (c) Schematic structure of the OPE-linked gold nanoparticle dimer trapped between the nanogap electrodes.

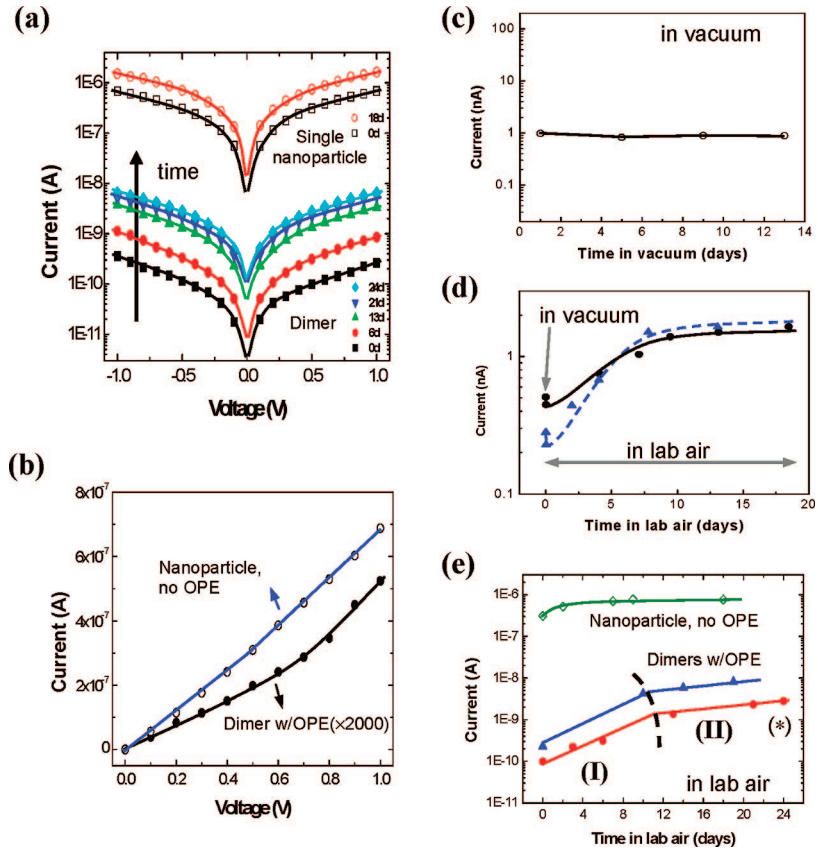

Figure 2. Ambient stability of the OPE-linked gold nanoparticle dimer trapped in the nanoscale electrode gap. (a) Several I−V curves for a typical nanoparticle/molecule/nanoparticle sample after various times exposed to air. The general shape of the I−V curve does not change upon air exposure. Also shown are I−V traces for single large (80 nm diameter) nanoparticles adsorbed in the nanogap (i.e., with no OPE molecules), showing significantly lower resistance than the nanoparticle/molecule dimers. (b) I−V curves showing the data from panel a on a linear scale, before exposure to air, emphasizing the different shape for the curves with and without the molecule present. (c) A molecular dimer device kept in vacuum shows no significant current change over more than 13 days. (d) Upon continuous air exposure, current through two different dimers is observed to show a rapid initial decrease, followed by a rapid increase over the next several days before transitioning to a slower rate of increase (measured at 0.5 V in air). (e) The current measured through three different dimers and one large nanoparticle (measured at 0.5 V in vacuum) exposed to ambient air for various times shows exponential increase in the current. The dashed line corresponds to an apparent change of the slope in log(current) versus time, delineating regions I and II. The line marked with an asterisk (*) corresponds to the data in panel a. All lines are drawn as a guide to the eye.

several days). Figure 2d shows the current measured through a dimer sample at 0.5V as a function of time exposed to air (and measured in air). The current showed a rapid initial decrease, followed by an increase over the next several days before transitioning to a slower rate of increase. Long et al.[3] analyzed the short-term ambient stability of conductance through thiol-terminated molecule ensembles using a magnetic microsphere bridge junction. They reported a rapid reversible decrease in conductance upon air exposure and ascribed the change to hydration of the thiolate moiety, leading to a disruption of the gold/sulfur bond. The initial decrease in the current shown in Figure 2d is consistent with the results and mechanisms presented by Long et al.

The remaining results presented here address the issue of long-term stability. The short-term current change upon the transition from air to vacuum or vacuum to air was not typically recorded. Figure 2e shows the current measured at 0.5 V plotted versus air exposure time for two dimer samples prepared using identical fabrication procedures. In this figure, the data points at day 0 correspond to the first measurements of each sample immediately after fabrication. Also shown in Figure 2e are results from the control experiment in which the current through the single gold nanoparticle was monitored in air as a function of time. The current through the gold nanoparticle was stable (within a factor of 2) upon exposure to air for up to 18 days, further indicating that the time-dependent current observed in the nanoparticle/molecule dimer was dominated by changes in the overall conductance through the molecular junction. We note that for the two example nanoparticle/molecule dimer structures in Figure 2e, the current measured immediately after junction formation exhibited some sample-to-sample variation. The data points shown represent the typical range of current values observed for the dimer samples we have measured to date. This variation likely reflects that some dimers may contain two or more molecules, that there is some variability in the metal/molecule contact structure within the dimer that affects the overall conductivity,[30] or both. Larger current values were observed in some samples and ascribed to defects or other contamination.

For each sample measured in air, the current shown in Figure 2e was observed to increase by a factor of 4−15 within the first 8−12 days of air exposure and then to continue to increase more slowly. We note that some dimer samples with higher initial current also showed the same behavior of current change with exposure to air. The data marked with an asterisk in Figure 2e correspond to the example I−V data set shown in Figure 2a. The initial rate of current increase with time was similar for all the devices measured and found to be proportional to $\sim\exp(t/\tau)$, where $\tau \approx 4.3$ is the characteristic time constant (in days) for the current increase. A dashed line in Figure 2e is drawn to

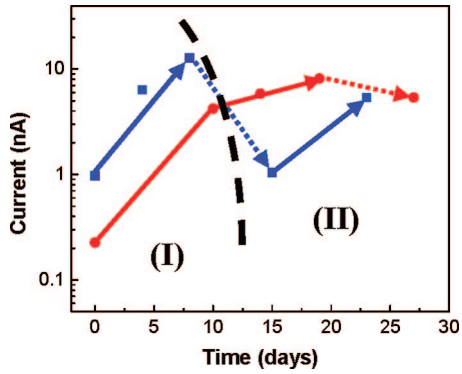

Figure 3. Current measured after various times in air (solid arrows) and after returning to desiccated vacuum storage for several days (dotted arrows). The thicker dashed line corresponds to the transition from region I to region II, as shown in Figure 2. For samples (■) exposed to air for relatively short times (i.e., still in region I), the current responds significantly to vacuum treatment, returning to nearly its original before-exposure value. Samples (●) exposed to air for a relatively long time (i.e., in region II) show less response to vacuum exposure. All lines are drawn as a guide to the eye.

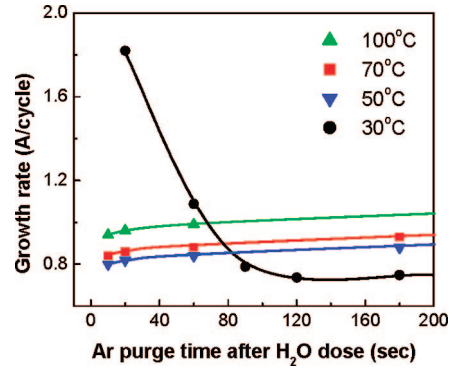

Figure 4. Atomic layer deposition growth rate of Al_2O_3 (in angstroms per ALD cycle) versus Ar purge time after the H_2O exposure step, at growth temperatures of 30−100 °C. At 30 °C, the growth rate of Al_2O_3 sharply decreased as the purge time increased from 20 to 120 s. All lines are drawn as a guide to the eye.

roughly delineate the regions for fast (region I) and slower (region II) current increases with time. We note that for the samples studied, the time required for the current to transition from a fast to a slower increase depends on the initial measured current such that devices with an initial smaller current require longer times for the current change to decrease, as compared to those with larger initial current values. The current stability was further evaluated by storing samples previously exposed to air in a desiccated vacuum ($\sim 10^{-2}$ Torr), then measuring the current after vacuum storage. Results are shown in Figure 3. For devices initially exposed to air for only a few days (i.e., current change was still in region I of Figure 2e), storing the samples in vacuum for several days resulted in a partial recovery (i.e., decrease) of current back to the initial pre-exposure value. However, devices exposed to air for many days (in region II in Figure 2e) exhibited a much smaller decrease in current after vacuum storage. This suggests that the long-term change in conductivity is somewhat reversible within the first few days, whereas the change becomes fixed or less reversible after longer-term (10−15 days) air exposure.

Generally, a molecular junction involves mixing between discrete orbitals in a molecule and the continuum states in a metal so that the metal/molecule/metal junction should be considered as a single unit. Instability mechanisms could include alterations of the molecule/metal linkage, the molecular electronic or physical configuration,[31] or both. The current measured as a function of air exposure time observed in Figures 2 and 3 showed that the current change of the molecule/nanoparticle dimer junction is much larger than for the nanoparticle/metal contact. One possible explanation for the change in conductance in the molecular junction is that contaminant species in air (i.e., water) adsorb in the junction region and increase the current. Contaminant adsorption can be expected to affect the molecule/nanoparticle junction as well as the nanoparticle/electrode connections. Any mechanical force that decreases the junction length by a small amount will also increase the magnitude of the tunneling current. For example, for an electron decay constant of 0.2−0.4 $Å^{-1}$, a 4−6 Å change in junction length would change the resistance by a factor of ∼5. Because of its large resistance, small modifications of the molecule junction will lead to a large change in measured conductivity, whereas small modification to the smaller resistance nanoparticle/electrode connections will show less change. The results in Figures 2 and 3 follow this trend. The partial reversibility and longer-term persistence of the instability upon subsequent vacuum exposure shown in Figure 3 are also consistent with contaminant condensation, where contaminant desorption from the nanoscale region between the nanoparticles becomes progressively more difficult with extended exposures.[32] Results shown here are not sufficient to uniquely identify the detailed mechanisms associated with the current instability.

We hypothesized that the instability of the molecular junctions could be improved by encapsulating the nanoparticle/molecule/nanoparticle dimer with an inert coating of a barrier dielectric film, such as Al_2O_3. Atomic layer deposition was chosen for these tests because it can be deposited at low temperature with high conformality. The low temperature will also allow minimal disruption of the gold−thiol bonded nanoparticle/OPE junction. Initially, ALD Al_2O_3 was carried out on planar silicon substrates for a range of ALD cycle numbers between 30 and 100 °C. Thickness was observed to increase linearly with the number of ALD cycles with a growth rate that increased from 0.74 to 0.99 Å/cycle as temperature increased from 30 to 100 °C when sufficiently long purge times were used after water exposure. Groner et al.[24] reported that for ALD Al_2O_3 at temperatures less than 100 °C, the rate of water molecule desorption from the growth surface had a significant effect on the growth rate. The data in Figure 4 show the effect of argon purge time, following the water exposure cycle, on the growth rate of Al_2O_3 at temperatures between 30 and 100 °C. The results show that the growth rate of Al_2O_3 was nearly independent of temperature between 50 and 100 °C. At 30 °C, the growth was strongly influenced by the Ar purge time after the H_2O exposure step, whereas at temperatures >50 °C, the growth rate was not significantly affected by the reactor purge time. For experiments performed here, long purge times were used, and growth conditions were fixed to achieve a similar film thickness (∼10 nm) at each temperature used.

To examine the conformality of the deposited coating, a nanoparticle dimer was placed on carbon support film and coated by the ALD method at 70 °C using 120 TMA/H_2O cycles, followed directly by evaluation with TEM. Figure 5a shows a TEM micrograph of the dimer after ALD treatment, revealing an Al_2O_3 coating with a thickness of ∼10 nm that is extremely uniform and conformal. The growth rate of Al_2O_3 film on gold nanoparticle dimer was calculated as ∼0.83 Å/cycle, equivalent to that observed on a Si substrate exposed to the same deposition conditions. This is due to the facile nucleation of Al_2O_3 film on the hydroxyl groups of the citrate capping layer covering the

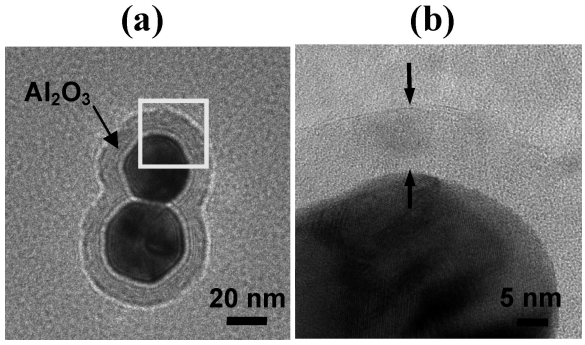

Figure 5. (a) TEM micrograph of an Al_2O_3-encapsulated, OPE-linked gold nanoparticle/molecule/nanoparticle dimer on a carbon support film on a copper TEM grid. (b) High-resolution TEM image of the inset region in panel a. An amorphous Al_2O_3 layer with a thickness of ~10 nm was deposited uniformly and conformally on the nanoparticle/molecule dimer.

gold nanoparticles. Figure 5b displays a high-resolution TEM image acquired near the interface between a gold nanoparticle and the Al_2O_3 layer, showing a distinction between the amorphous Al_2O_3 film and the polycrystalline gold nanoparticle.

A series of current-versus-voltage measurements was carried out for samples coated with ALD Al_2O_3 immediately after coating and over several days of continuous air exposure; the results are shown in Figure 6. The data collection protocol followed the methods used for collecting data for uncoated samples in Figure 2. Figure 6a shows a set of I−V curves for one example junction coated at 50 °C, including an I−V trace made immediately after junction formation and before ALD coating as well as traces collected over a range of times after coating. Generally, the shape of the I−V traces was not affected by the ALD coating procedure. The current at 0.5 V measured for four dimer samples before and after ALD treatment at temperatures between 30 and 100 °C is shown in Figure 6b. Similar to the data in Figure 2e, the data from four dimer samples in Figure 6b show sample-to-sample variation in the conductivity measured immediately after junction formation. After coating, all samples were exposed to air, similarly to the samples shown in Figure 2, and the I−V data were collected at various times after air exposure. Samples measured immediately after coating showed conductivity values larger than the original precoating values, and the magnitude of change became more pronounced as the ALD temperature was increased. For all dimer samples, the current after coating decreased slowly over 1−2 days then stayed relatively stable during analysis as long as 19 days. The samples encapsulated at 30 and 50 °C show similar behavior in that the current after encapsulation stabilizes at a value within a factor of ~2 of the original value measured before encapsulation. The data points at 50 °C correspond to the data shown in Figure 6a.

It is important to note that when the current through these ALD encapsulated samples was measured in real time during a vacuum-to-air or air-to-vacuum transition, the current remained unchanged, whereas uncoated samples observed by our group and by Long et al.[3] showed a rapid decrease in current upon air exposure. The ALD process included exposing the samples to vacuum (~10^{-6} Torr) at the deposition temperature (30 to 100 °C) for approximately 30 min before deposition was initiated. When the ALD encapsulation was performed at higher temperatures, 70 and 100 °C, the current increased by a factor of 10−100 or more, and the current remained high after extended measurement times. In Figure 6c, the net change in measured current is shown as a function of processing temperature. For

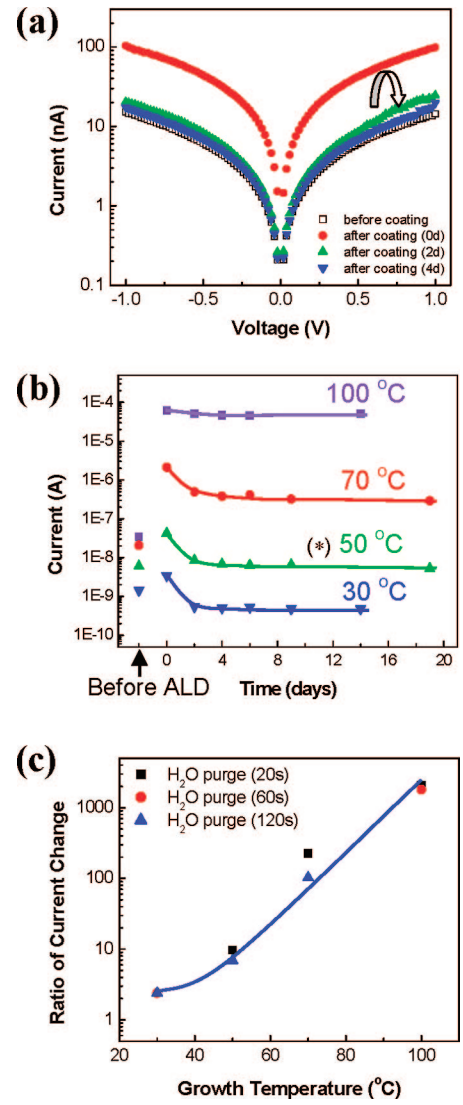

Figure 6. (a) Typical I−V curves for a nanoparticle/molecule/nanoparticle dimer after coating with ALD Al_2O_3 at 50 °C using a deposition rate of ~0.8 Å/cycle. (b) The current measured through four different devices (measured at 0.5 V in vacuum) exposed to ambient air for various times, with ALD Al_2O_3 encapsulation deposition performed at various temperatures. The data marked with an asterisk correspond to the data shown in panel a. The data point at time = 0 corresponds to the current measured in vacuum immediately after encapsulation. The samples with the low-temperature Al_2O_3 encapsulation layer showed stable current at a value similar to the precoating value. (c) Net current change of the encapsulated dimer (measured at 0.5 V in vacuum) as a function of Al_2O_3 deposition temperature. Various Ar purge times after H_2O exposure were used. Lines are drawn as a guide to the eye.

all I−V traces collected from the dimer samples, the curves showed nonlinear I−V traces consistent with nonresonant charge tunneling before and after ALD treatment.

A few samples were treated with ALD at 200−230 °C, and after deposition the samples showed very high current that was linear with voltage, consistent with shorting of the nanoparticles and irreversible degradation of the molecular junction. Two samples with electrodes bridged by only one large nanoparticle (i.e., with no molecule junction) were also coated by ALD at 50 and 100 °C. In both samples, the current increased by a factor of 10 or more after deposition, indicating improved nanoparticle/electrode contact after ALD treatment.

As a further control experiment, the specific effects of the various ALD reactants and procedures on the current through

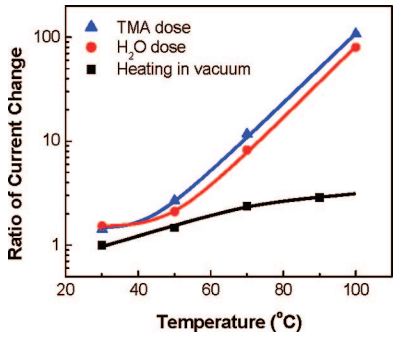

Figure 7. Effect of H_2O and TMA exposure and vacuum thermal treatment at 30−100 °C on the current change (at 0.5 V) through 12 nanoparticle dimer samples. The ratio corresponds to the current after treatment divided by the current before treatment. All currents are measured after sample cooling to room temperature.

the molecular junction were individually investigated in the ALD furnace at 30−100 °C and 0.5 Torr. Specifically, samples were exposed to one of three treatments: (i) water vapor and argon (consisting of 0.3 s of H_2O followed by 120 s of Ar for 20 cycles); (ii) trimethylaluminum vapor and argon (consisting of 1.0 s of TMA followed by 20 s of Ar for 20 cycles); or (iii) heating in vacuum for times equal to the duration of a typical ALD process. None of these exposure sequences resulted in film deposition under the conditions studied. Current-vs-voltage characteristics were measured, and the ratio of current (at 0.5 V) measured before and after treatment was plotted as shown in Figure 7. All treatments at $T > 50$ °C were observed to affect the current through the junction, whereas none of the treatments had significant affects on the junction properties when performed at $T \leq 50$ °C.

Samples exposed to heating in vacuum also showed relatively small changes. Although the results presented here cannot unambiguously determine the mechanisms associated with the observed current instability, the results in Figure 7 show clearly that exposing the junctions to TMA or water vapor under vacuum (0.5 Torr) and temperature conditions (30−50 °C) for short times (seconds) typical of low-temperature ALD does not significantly degrade molecular junction conductivity or tunneling performance. Trimethylaluminum is highly reactive, but the relative insensitivity of the junction to the TMA exposure under the conditions used may result from the geometrical constraints of the system. Specifically, a molecule ~2 nm in length connected to two 40-nm-diameter nanoparticles creates a very small gap region between relatively large nanoparticles, and reactive species diffusing into this region are likely to collide and react with a partially oxidized or coated nanoparticle surface well before reaching the small molecule at the center of the junction. Moreover, Elam et al.[33] report that aromatic molecules show relatively low reactivity to ALD Al_2O_3 deposition reactions. Furthermore, any reaction between the citrate on the nanoparticle and the TMA will help impede TMA from reaching the active molecule.

To confirm the presence of the molecular junction after ALD encapsulation, several experiments were performed; the results are shown in Figure 8. The junction before and after ALD coating measured up to 2 V shows similar behavior in Figure 8a. Another coated junction measured from 0 to 10 V showed high current spikes near 5−6 V, consistent with junction breakdown and a transition to current flow through the oxide coating.[35] The same junction after the high-voltage treatment shows much lower current at low voltage, consistent with junction loss. AFM analysis of the nanogap region provides

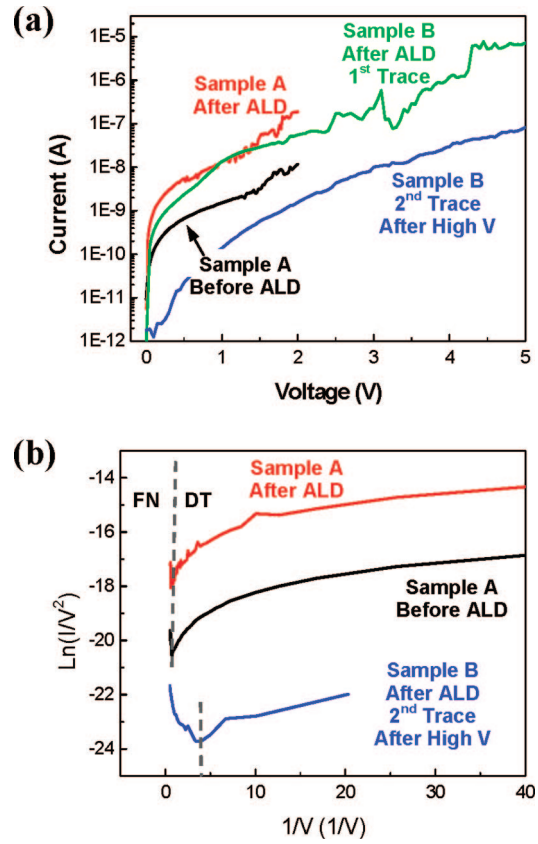

Figure 8. (a) I−V characteristics of molecular junctions, including one sample measured before and after ALD between 0 and +2 V and another sample measured up to 5 V applied bias. Up to 2 V applied bias, the I−V trace is generally reproducible for many measurement cycles. After exposure to high field, the I−V trace shows a significantly reduced current, consistent with loss of the molecular junction. (b) A plot of $\ln(I/V^2)$ vs $1/V$ shows the transition from direct to Fowler−Nordheim tunneling for uncoated and coated samples and for a coated sample after high-field treatment. The transition field does not change upon ALD encapsulation, but it changes significantly after high-field treatment. Results indicate that the molecular junction is intact after ALD encapsulation and is lost only during high-field exposure.

evidence that the dimers are still present in the gap after breakdown, giving credence that the molecule junction is present after ALD (before breakdown). Furthermore, the transition from direct to Fowler−Nordheim tunneling is characterized before and after ALD encapsulation, and the transition voltage, determined from the change in slope of a plot of $\ln(I/V^2)$ vs $1/V$ (Figure 8b), is the same before and after encapsulation.[16,34] Loss of the molecule junction is expected to lead to significant change in the tunnel junction barriers and a change in the transition voltage between direct and Fowler−Nordheim tunneling,[16,34] consistent with results in Figure 8b. These results support the presence of the OPE molecules after ALD Al_2O_3 coating.

Several mechanisms could account for the initial increase in current observed after ALD and the subsequent decrease in current during the first 1−2 days after encapsulation. Considering first the larger current measured after encapsulation, as shown above, the current through the junction is expected to increase upon exposure to laboratory air. The sample transfer from the I−V measurement chamber to the ALD reactor proceeds through laboratory air. Therefore, exposure to laboratory air during sample transfer, loading, and pump-down in the ALD reactor system could affect the junction conductivity. In addition, data in Figure 7 indicate that sample heating and water

exposure during the ALD process will also increase junction conductance. Other mechanisms could account for the current decrease after ALD encapsulation. For example, the Al_2O_3 deposited at low temperature is not as dense as that deposited at high temperatures, so it is possible that water or other contaminants originating in the deposited film may be contributing to the instability for 1−2 days after coating.

The data presented here show that the current through a molecular junction containing a single or small number of molecules is sensitive to ambient exposure over short and long exposure times. Although the results shown here cannot explicitly identify the mechanisms associated with the current instability, reasonable arguments can be made to account for the observed trends, including the effects of ambient water or other contaminants. Results show that exposing molecular junctions to atomic layer deposition processes at low temperatures (≤50 °C) to form Al_2O_3 encapsulating layers around the molecule junctions, the junction conductance is not significantly modified by the deposition process itself. Moreover, junctions coated at low temperature show significantly improved long-term stability, during which the molecular conductance does not change during storage for more than 20 days in laboratory air. This encapsulation method can be used, for example, to stabilize junctions for extended analysis and functional evaluation. Further work can probe the detailed effects of the ALD process on the structure of the oligomeric phenylene ethynylene molecule or molecules in the dimer junction. Furthermore, this work provides a new route for gentle encapsulation and stabilization for a variety of synthetic molecule/nanoparticle structures and other engineered molecular nanosystems.

Experimental Methods

Nanoparticle/Molecule/Nanoparticle Fabrication and Electrical Contact Formation. To form the dimers, OPE structures terminated with thioacetate functionalities were bridged by two ∼40 nm gold nanoparticles (citrate-capped, Ted Pella, Inc.) after in situ deprotection of the acetyl group.[16] A stoichiometric amount of the OPE molecules was mixed with the solution containing gold nanoparticles, which maintains their respective ratio of 1:2, to avoid aggregate formation. The TEM image of an uncoated dimer in Figure 1a was obtained with a Philips CM12 TEM operated at 100 kV, where images were captured using a Gatan 780 camera and Digital Micrograph software. TEM was also used to evaluate the statistical distribution of synthesized nanoparticles. For ∼173 items counted, 62% were isolated particles, 31% were bound in dimers, and 7% were formed as trimers (i.e., three nanoparticles bound together). The plan-view SEM image in Figure 1b was collected at a magnification of 120 000 using Hitachi S-3200 with an accelerating voltage of 30 kV. Trapping of OPE-linked gold nanoparticle dimers was performed in the probe station by placing a ∼3 μL droplet of the dimers suspended in aqueous solution onto the electrode surface. For dielectrophoretic trapping, an alternating current electric field was applied to the electrodes.[13,15] The voltage was typically ∼1−3 VAC at a frequency of 1 KHz to 1 MHz for 20−120 s. After trapping, samples were rinsed in deionized water for 30 s and dried in a stream of nitrogen gas. The best conditions for dielectrophoretic trapping of dimers were observed to be 2 VAC, 1 MHz, and 60 s, at which point successful trapping of 51 devices out of 58 experimental trials (i.e., success rate of ∼88%) was achieved. In this case, success is achieved when a reasonably self-consistent current level (i.e., not shorted and not open) is measured after trapping. Typically, AFM analysis shows one to three dimers trapped in the electrode nanogap. The AC voltage was generated using a precision LCR meter (Agilent 4284A) that is computer-controlled using LabView from National Instruments. Further details of the nanogap electrode fabrication procedure and the assembly of dimers within them are described elsewhere.[16]

Atomic Layer Deposition and Film Characterization. Atomic layer deposition of Al_2O_3 was performed using trimethylaluminum (TMA, $Al(CH_3)_3$) and deionized water as precursor and oxidant gas, respectively. Argon was used as a carrier and purge gas. The deposition was carried out in a home-built, hot-wall quartz tube reactor. TMA was obtained from STREM Chemicals and used as received. Argon gas was purified using a Drierite gas purifier to remove possible moisture and impurities from the gas line. One typical reaction cycle of ALD consists of TMA dose (1 s)/Ar purge (20 s)/H_2O dose (0.3 s)/Ar purge (20−120 s). Samples were exposed to a vacuum of $\sim 10^{-6}$ Torr for 30 min to obtain a uniform temperature distribution in the reaction chamber before ALD coating. The growth temperature ranged from 30 to 100 °C, and the operating pressure was maintained at 0.5 Torr with a total gas flow rate of 100 sccm. The control volume was used to supply a constant amount of a precursor and oxidant gas during each cycle.

After deposition, the film thickness of Al_2O_3 on planar silicon substrates was measured using an Auto EL ellipsometer (Rudolph Tech.) at an angle of incidence of $\Phi = 70°$ and a wavelength of $\lambda = 632.8$ nm. To characterize and examine conformality of the Al_2O_3 coatings on the dimer structures, several OPE-linked gold nanoparticle dimers were placed on a carbon support film on a copper grid (carbon type A obtained from Ted Pella, Inc.) The TEM copper grid was initially baked at ∼120 °C for at least 10 min, followed by addition of several drops of the solution containing the nanoparticle/molecule/nanoparticle dimers. Grids with dimers were placed into a vacuum desiccator ($\sim 10^{-2}$ Torr) overnight, followed by ALD treatment. For these samples, TEM analysis was carried out with a JEOL 2010F high-resolution TEM operated at 200 kV using a Schottky field emitter in combination with electron energy loss spectroscopy.

Current-vs-Voltage Analysis. For the dimers adsorbed onto the nanogap electrodes, the current−voltage measurements were performed in a vacuum-compatible probe station (Janis Research Co., Inc.) using a Keithley 2602 sourcemeter, and heating was carried out using a 331 temperature controller (LakeShore). When not being measured, samples were generally stored in the dark in a vacuum desiccator in the milli-Torr pressure range with no bias applied. Some samples were stored in laboratory ambient air, also without applied bias and isolated from visible light exposure. For each measurement, samples were transferred in air to the vacuum probe station. Unless specifically noted, current-vs-voltage measurements were performed under a vacuum of $\sim 5 \times 10^{-4}$ Torr. The total time for each sample analysis point, including sample transfer, pumping, and multiple I−V measurements (typically three to five times for each sample) was ∼1−2 h. After measurements, the samples were transferred in air to storage (in air or vacuum) until the next analysis point was collected.

Acknowledgment. The authors acknowledge support from the National Science Foundation, awards DMR 0303746 and CTS 0626256.

References and Notes

(1) Lee, M. T.; Hsueh, C. C.; Freund, M. S.; Ferguson, G. S. Air oxidation of self-assembled monolayers on polycrystalline gold: The role of the gold substrate. *Langmuir* **1998**, *14*, 6419–6423.

(2) Schoenfisch, M. H.; Pemberton, J. E. Air stability of alkanethiol self-assembled monolayers on silver and gold surfaces. *J. Am. Chem. Soc.* **1998**, *120*, 4502–4513.

(3) Long, D. P.; Lazorcik, J. L.; Mantooth, B. A.; Moore, M. H.; Ratner, M. A.; Troisi, A.; Yao, Y.; Ciszek, J. W.; Tour, J. M.; Shashidhar, R. Effects of hydration on molecular junction transport. *Nat. Mater.* **2006**, *5*, 901–908.

(4) Akkerman, H. B.; Blom, P. W. M.; de Leeuw, D. M.; de Boer, B. Towards molecular electronics with large-area molecular junctions. *Nature* **2006**, *441*, 69–72.

(5) Selzer, Y.; Allara, D. L. Single-molecule electrical junctions. *Annu. Rev. Phys. Chem.* **2006**, *57*, 593–623.

(6) Chen, F.; Hihath, J.; Huang, Z. F.; Li, X. L.; Tao, N. J. Measurement of single-molecule conductance. *Annu. Rev. Phys. Chem.* **2007**, *58*, 535–564.

(7) Reichert, J.; Ochs, R.; Beckmann, D.; Weber, H. B.; Mayor, M.; von Lohneysen, H. Driving current through single organic molecules. *Phys. Rev. Lett.* **2002**, *88*, 176804.

(8) Selzer, Y.; Cabassi, M. A.; Mayer, T. S.; Allara, D. L. Thermally activated conduction in molecular junctions. *J. Am. Chem. Soc.* **2004**, *126*, 4052–4053.

(9) Keane, Z. K.; Ciszek, J. W.; Tour, J. M.; Natelson, D. Three-terminal devices to examine single-molecule conductance switching. *Nano Lett.* **2006**, *6*, 1518–1521.

(10) Cui, X. D.; Primak, A.; Zarate, X.; Tomfohr, J.; Sankey, O. F.; Moore, A. L.; Moore, T. A.; Gust, D.; Harris, G.; Lindsay, S. M. Reproducible measurement of single-molecule conductivity. *Science* **2001**, *294*, 571–574.

(11) Donhauser, Z. J.; Mantooth, B. A.; Kelly, K. F.; Bumm, L. A.; Monnell, J. D.; Stapleton, J. J.; Price, D. W.; Rawlett, A. M.; Allara, D. L.; Tour, J. M.; Weiss, P. S. Conductance switching in single molecules through conformational changes. *Science* **2001**, *292*, 2303–2307.

(12) Xu, B. Q.; Tao, N. J. Measurement of single-molecule resistance by repeated formation of molecular junctions. *Science* **2003**, *301*, 1221–1223.

(13) Amlani, I.; Rawlett, A. M.; Nagahara, L. A.; Tsui, R. K. An approach to transport measurements of electronic molecules. *Appl. Phys. Lett.* **2002**, *80*, 2761–2763.

(14) Long, D. P.; Patterson, C. H.; Moore, M. H.; Seferos, D. S.; Bazan, G. C.; Kushmerick, J. G. Magnetic directed assembly of molecular junctions. *Appl. Phys. Lett.* **2005**, *86*, 153105.

(15) Dadosh, T.; Gordin, Y.; Krahne, R.; Khivrich, I.; Mahalu, D.; Frydman, V.; Sperling, J.; Yacoby, A.; Bar-Joseph, I. Measurement of the conductance of single conjugated molecules. *Nature* **2005**, *436*, 677–680.

(16) Na, J.-S.; Ayres, J.; Chu, C.; Chandra, K.; Gorman, C. B.; Parsons, G. N. Conduction mechanisms and stability of single molecule nanoparticle/molecule/nanoparticle junctions. *Nanotechnology* **2007**, *18*, 035203.

(17) Chu, C.; Na, J.-S.; Parsons, G. N. Conductivity in alkylamine/gold and alkanethiol/gold molecular junctions measured in molecule/nanoparticle/molecule bridges and conducting probe structures. *J. Am. Chem. Soc.* **2007**, *129*, 2287–2296.

(18) Hakim, L. F.; George, S. M.; Weimer, A. W. Conformal nanocoating of zirconia nanoparticles by atomic layer deposition in a fluidized bed reactor. *Nanotechnology* **2005**, *16*, S375−S381.

(19) Lee, J. S.; Min, B.; Cho, K.; Kim, S.; Park, J.; Lee, Y. T.; Kim, N. S.; Lee, M. S.; Park, S. O.; Moon, J. T. Al_2O_3 nanotubes and nanorods fabricated by coating and filling of carbon nanotubes with atomic-layer deposition. *J. Cryst. Growth* **2003**, *254*, 443–448.

(20) Herrmann, C. F.; Fabreguette, F. H.; Finch, D. S.; Geiss, R.; George, S. M. Multilayer and functional coatings on carbon nanotubes using atomic layer deposition. *Appl. Phys. Lett.* **2005**, *87*, 123110.

(21) Yun, S. J.; Ko, Y. W.; Lim, J. W. Passivation of organic light-emitting diodes with aluminum oxide thin films grown by plasma-enhanced atomic layer deposition. *Appl. Phys. Lett.* **2004**, *85*, 4896–4898.

(22) Ghosh, A. P.; Gerenser, L. J.; Jarman, C. M.; Fornalik, J. E. Thin-film encapsulation of organic light-emitting devices. *Appl. Phys. Lett.* **2005**, *86*, 223503.

(23) Puurunen, R. L. Surface chemistry of atomic layer deposition: A case study for the trimethylaluminum/water process. *J. Appl. Phys.* **2005**, *97*, 121301.

(24) Groner, M. D.; Fabreguette, F. H.; Elam, J. W.; George, S. M. Low-temperature Al_2O_3 atomic layer deposition. *Chem. Mater.* **2004**, *16*, 639–645.

(25) Nuzzo, R. G.; Zegarski, B. R.; Dubois, L. H. Fundamental studies of the chemisorption of organosulfur compounds on Au(111)−implications for molecular self-assembly on gold surfaces. *J. Am. Chem. Soc.* **1987**, *109*, 733–740.

(26) Chechik, V. Reduced reactivity of aged Au nanoparticies in ligand exchange reactions. *J. Am. Chem. Soc.* **2004**, *126*, 7780–7781.

(27) Brousseau, L. C.; Novak, J. P.; Marinakos, S. M.; Feldheim, D. L. Assembly of phenylacetylene-bridged gold nanocluster dimers and trimers. *Adv. Mater.* **1999**, *11*, 447–449.

(28) Blum, A. S.; Kushmerick, J. G.; Pollack, S. K.; Yang, J. C.; Moore, M.; Naciri, J.; Shashidhar, R.; Ratna, B. R. Charge transport and scaling in molecular wires. *J. Phys. Chem. B* **2004**, *108*, 18124–18128.

(29) James, P. N. Synthesis, optical and electronic investigations of organically bridged metal nanoparticle arrays. PhD thesis, North Carolina State University, Raleigh, 2001.

(30) Hu, Y. B.; Zhu, Y.; Gao, H. J.; Guo, H. Conductance of an ensemble of molecular wires: A statistical analysis. *Phys. Rev. Lett.* **2005**, *95*, 156803.

(31) Lindsay, S. M.; Ratner, M. A. Molecular transport junctions: Clearing mists. *Adv. Mater.* **2007**, *19*, 23–31.

(32) Kim, S.; Ehrman, S. H. Capillary condensation onto titania (TiO_2) nanoparticle agglomerates. *Langmuir* **2007**, *23*, 2497–2504.

(33) Elam, J. W.; Wilson, C. A.; Schuisky, M.; Sechrist, Z. A.; George, S. M. Improved nucleation of TiN atomic layer deposition films on SILK low-k polymer dielectric using an Al_2O_3 atomic layer deposition adhesion layer. *J. Vac. Sci. Technol. B* **2003**, *21*, 1099–1107.

(34) Beebe, J. M.; Kim, B.; Gadzuk, J. W.; Frisbie, C. D.; Kushmerick, J. G. Transition from direct tunneling to field emission in metal−molecule−metal junctions. *Phys. Rev. Lett.* **2006**, *97*, 026801.

(35) Groner, M. D.; Elam, J. W.; Fabreguette, F. H.; George, S. M. Electrical characterization of thin Al_2O_3 films grown by atomic layer deposition on silicon and various metal substrates. *Thin Solid Films* **2002**, *413*, 186–197.

JP8066298